The Bioscan
AN INTERNATIONAL QUARTERLY JOURNAL OF LIFE SCIENCES
20(1): 568-582, 2025 www.thebioscan.com

Sustainable Fabrication of TiO_2 Nanoparticles: For Enhanced Cytotoxicity and Photocatalytic Efficiency

Avinash Ashok Survase [a] *, Avdhut Dadaso Kadam[b], Bandu Shamlal Pawar[a], Amol Sheshrao Jadhav[a], Nilesh Tukaram Pandit[b], Shivangi Shivraj Kanase[a] *

[a]Department of Microbiology, Yashavantrao Chavan Institute of Science, Karmaveer Bhaurao Patil University, Satara, 415 001, INDIA

[b]Department of Chemistry, Yashavantrao Chavan Institute of Science, Karmaveer Bhaurao Patil University, Satara, 415 001, INDIA

***Corresponding Author:** surwasedada09@gmail.com (**Dr. Avinash Ashok Survase**)

DOI: https://doi.org/10.63001/tbs.2025.v20.i01.pp568-582

KEYWORDS
Kaas Lake,
Titanium dioxide,
Nanospheres,
Bioremediation,
Anticancer study

Received on:
04-01-2025

Accepted on:
04-02-2025

Published on:
11-03-2025

ABSTRACT

Kaas plateau isolated *Bacillus halodurans* bacteria used for synthesis of TiO_2 NPs. The NPs show maximum absorbance at 384 nm. The functional groups of biomolecules play significant role in capping and stabilization of NPs. XRD indicates pure anatase tetragonal crystal nature of NPs. TEM show spherical morphology of TiO_2 material having mean diameter 33 nm. Brunauer-Emmett-Teller (BET) indicates a large specific surface area 13.0665 m^2/g with mesoporous nature. TiO_2 NPs exhibiting 99% degradation performance of diazo dye Red HE3B within 30 min and 92% MDA-MB-231 breast cancer cell growth inhibitory activity. Degradation pathway of Red HE3B was predicted on basis of LC-MS. Phytotoxicity of degraded metabolites showed enhanced growth of seedlings. TiO_2 NPs showed enhanced anticancer activity against human breast cancer cell line MDA-MB-231 tumour cells with 56.41 µg/ml IC_{50} value.

INTRODUCTION

Development in the sector of nanobiotechnology leads to the revolution in the fields of agriculture and industrial sectors enhancing effortless life of human beings and increasing living standard of human life. Textile industry is one of the rapidly expanding sectors in 21st century. Before mid-19th century dyes were derived from natural sources only. The growing population, increasing demand and excessive costs of natural dye extraction techniques, lead to the discovery of alternative source of dye. Perkin chemist was discover the first artificial synthetic dye aniline in 1856 [1] followed by unlimited discovery of different types of dyes. Azo dyes are most prominent groups, used in textile industries.

Red HE3B which is highly photolytically stable diazo dye and requiring more time for degradation was selected for our work. The direct interaction of diazo dyes creates serious issues in human life and creates various disorders [2] [3]. In addition, prolonged exposure to azo dyes may result in mutation in DNA or uncontrolled growth cells called cancer. In 2020, 10 million cancer deaths were recorded in the world [4], breast cancer is the most commonly encountered tumor, which causes around 23% of female fatalities every year. This type of cancer is extremely heterogeneous encompassing a group of genetically and epigenetically distinct diseases [5]. There are few treatments available to stop breast cancer cell proliferation. MDA-MB-231 vitro cells are utilized for the study of anticancer activity. We have addressed our work taking into consideration these two environmental and medically related major issues [6].

In the field of photocatalysis and anticancer activity, nanoscale transition metal oxide semiconductors (TMOS) play a crucial role due to high surface-to-volume ratio, appropriate optical band gap, chemical and photo stability, and many others properties. In recent years a lot of reports have been published on the microbial synthesis of gold, silver, iron, copper, and various nanoscale MOS such as TiO_2, V_2O_5, WO_3, and ZnO NPs [7, 8]. Among various metallic NPs, we decided to work with TiO_2 material because of their multidisciplinary applications in various fields [9]. TiO_2 NPs show excellent photocatalytic performance by oxidation reduction mechanism [10].

TiO_2 NPs also receive more awareness due to their optimize band gap, low cost, amphoteric nature, high specific resistivity, low toxicity, and small size, so they can penetrate through small size capillaries up to cells and permit effective drug delivery and activity at specific target site [11, 12] they also finds applications in bone tissue-repair engineering, antimicrobial activity, anticancer therapy, bone therapies, dentistry, cardiovascular stents, and many other therapies that required an implantable device [13].

In the present work, biosynthesized TiO_2 NPs enhance the formation of ROS in sunlight irradiation, aiding in efficient photocatalytic degradation of environmental pollutants of Red HE3B diazo dye. The effects of several parameters such as pH, catalyst concentrations, rpm, time and concentrations of dye on the degradation have also been studied and analysis of degraded metabolites. Degraded metabolites exhibit reduced toxicity and increase growth stimulation in seeds. TiO_2 is found to exhibit effective cytotoxic potential against MDA-MB-231 cancer cells. We claim, TiO_2 NPs synthesized by isolated *Bacillus halodurans* as a new potential candidate for textile dye bioremediation & anticancer agent.

2. Materials and methods

2.1. Chemicals

Titanium tetraisopropoxide (TTIP), HPLC grade methanol, Na_2SO_4, ethyl acetate, Red HE3B textile dye were purchased from Sigma Aldrich USA. Sabouraud dextrose broth and agar powder was purchased by Hi-Media Company.

2.2. Microorganism isolation and nanomaterial synthesis

The Avinash and co-workers reported methodology was used for isolation of microorganism. Ten bacterial strains were isolated. The microbial biosynthesis technique used for TiO_2 NPs formation. All isolated ten bacterial strains are challenged with 10^{-3} M Ti precaursor salt. The reaction was done for 24 h. In ten bacterial culture only one bacteria exhibited promising results [14].

2.3. Characterization of Material

The UV-Vis spectrum of nanomaterial was monitored using Double beam monochromator UV-2700i equipped with Integrating Sphere Attachment assembly (ISR-2600/ISR-2600Plus) Shimadzu. The FTIR-7600 λ instrument used for identifies functional groups in nanomaterials. Crystallographic and phase of NPs monitored using powder X-ray diffraction (XRD) technique. The transmission electron microscopy (TEM) used for fine scale image observation of NPs. Synthesized NPs specific surface area was analysed by using Brunauer-Emmett-Teller (BET).

2.4. Red HE3B dye degradation using Photocatalytic experiment

For Photocatalytic dye degradation, 10 mg dye and 1 mg TiO_2 mixed in 100 ml distilled water. The same concentration dye solution without NPs was kept as control. The catalyst mixed dye solution was illuminated sunlight radiation. From mixture of solution (5ml) sample were withdrawn equal time interval (10 min) and separate TiO_2 NPs by centrifugation. UV-Vis spectroscopy used for record absorbance spectra of NPs free supernatant. The percentage of dye degradation was estimated using the degradation percentage equation [15].

2.5. Degraded dye analysis

The dye degradation was confirmed using different spectroscopic techniques. UV-Visible dual beam spectroscopy was used for UV-Vis spectroscopic analysis. The degraded dye dried residues of sample were analyzed by various analytical techniques. FTIR analysis was done using single-beam spectrophotometer instrument. HPLC characterization was carried out using double beam absorbance detector containing C-18 column (4.6×250mm). The dried sample was dissolved in mobile phase for LC-MS analysis. TLC was done using silica gel act as stationary phase and methanol:distilled water (9:1) proportion as mobile phase.

2.6. Cell line

The MDA-MB-231 cell line was used for cytotoxicity test. Maintain pure cell lines in Dulbeccos modified Eagle medium (DMEM) high glucose media with 10% Fetal bovine serum (FBS) and antimycotic antibiotic solution 1% in the 5% CO_2, 18-20% O_2 atmosphere at 37 °C with CO_2 incubator, subculturing of pure cultures for every 2 days.

2.6.1. MTT Assay

The colorimetric assay used for study the cytotoxicity effect of TiO_2 NPs on cancerous cells. The live cells produces enzyme mitochondrial lactate dehydrogenase is key component for reduction of MTT dye into non soluble formazan crystals. The spectrophotometer used to measure cell viability. The cultured MDA-MB-231 cells (2 × 10^4/well) in 96 flat-base well plates and incubated in humidified conditions for 24 h at 37 °C allow to cell grow. After 24 h incubation period, The biosynthesized TiO_2 NPs were challenged with different concentrations (25, 50, 100, 200 and 300 µg/ml) against MDA-MB-231 cells, control cells maintained without any concentration of NPs. Incubate all plates for 48 h at 37°C in a 5% CO_2 atmosphere. The phosphate buffer saline solution was used for washing of cells and then added (3-(4,5-dimethylthiazol-2-yl)-2,5-diphenyltetrazolium bromide (MTT) dye to prepare final concentration of 0.5 mg/mL of total volume. Then cover the sample plates with aluminium foil to avoid exposure of light radiation and incubate plates for 3 h. The insoluble purple formazon crystals were dissolved in 100 µl dimethyl sulfoxide (DMSO) and stirring on shaker to increase solubility. Estimate the absorbance spectrum on UV-Visible spectroscopy or an ELISA reader (ELX-800, BioTeK, USA) at 570 nm wavelength with reference microplate reader. The 50% of inhibition of cells viability is calculated using the following equation [16].

$$\%\ of\ inhibition = \frac{Absorbace\ of\ untreated\ cells - Absorbance\ of\ treated\ cells}{Absorbace\ of\ untreated\ cells}\ x\ 100 \quad ......(1)$$

2.6.2. Microscopic study

The inverted biological (Biolinkz) microscope used to examine the MDA-MB-231 cells' size, shape, and cell-cell adhesion in cellular crowding. Photographs of each well MDA-MB-231 cell's treated with NPs and untreated control samples were captured at a 20x magnification using the Biolinkz view imaging software.

3. Results and discussion

3.1. Synthesis of TiO_2 NPs

The colour change and precipitate formation was visualized in screw cap bottle containing extracellular fungus extract reacted with 10^{-3}M titanium tetraisopropoxide within 24 h at 37°C, 120 rpm. When CFE reacted with precursor TTIP observation of whitish precipitate demonstrated role of biomolecules in CFE in synthesis of TiO_2 NPs. **Fig. 1 (a)** shown a diagrammatic presentation of the biological synthesis of pure anatase TiO_2 NPs using Kaas lake isolated, 16S-rRNA sequencing identified *Bacillus halodurans* bacterial extract [17].

Fig.1- (a)- Schematic representation of biosynthesis of TiO_2 NPs using microorganism

3.2. Characterization of the TiO_2NPs

3.2.1. UV-Vis DRS

UV-Vis DRS analysis use to study the optical properties and kinetic formations of TiO_2 NPs.The anatase TiO_2 NPs, show Ti^{+4} is surrounded by six oxygen atoms in an octahedral coordination, forming octahedral complex TiO_6[18]. The sharp visual UV-Vis DRS spectrum of white precipitate TiO_2 NPs observed at about 384 nm within 48 h at 37 °C, 140 rpm shown in **Fig. 2 (a).** The transfer charge from the valence band formed by the 2p orbitals of the oxide anions to the conduction band generated by the 3d t_{2g} orbitals of the Ti^{+4} cations. The TiO_2 show maximum absorbance at range 200-400 nm is due charge translocation between two bands. The strong absorption at $\lambda < 400$ nm, revealing production of TiO_2 NPs [19], the exact position may fluctuate due to various dimensions such as size and shape of NPs [14].

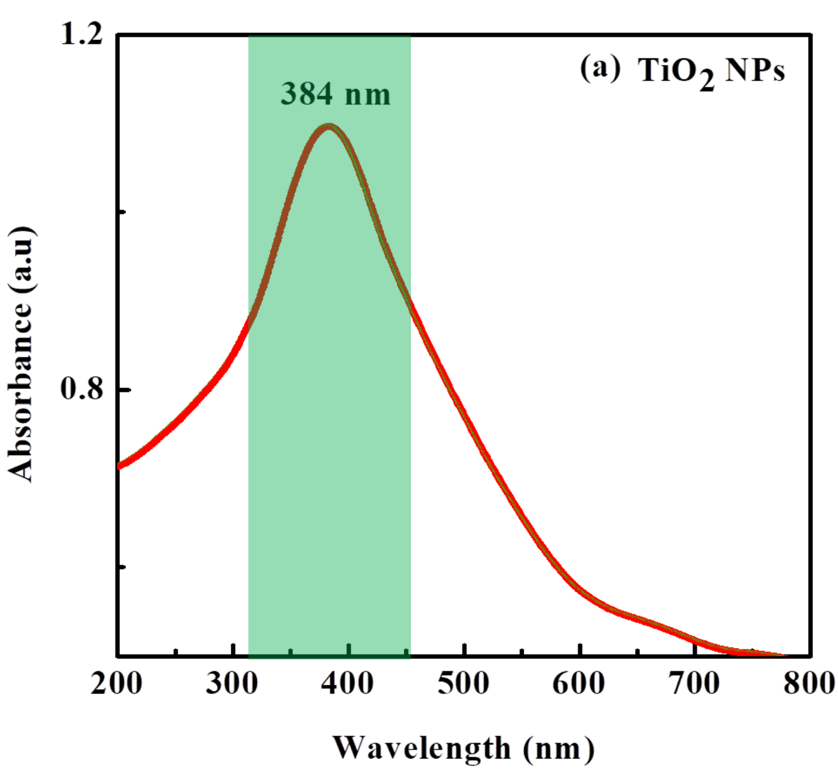

Fig. 2 (a) UV-vis absorption Spectrum of TiO_2 nanoparticles

The TiO_2 shown greater than 3 eV band gap. TiO_2 anatase phase reduces the light absorption, which may rise the valence band maxima to more energy levels relative to redox potentials of molecules that adsorbed. This leads to enhnace the oxidation 'potetial' of electrons and facilitates electron shifting from the TiO_2 to adsorbed molecules [20].The optical bandgap of calcinated product can be calculated using Tauc relation. **Fig. 2 (b)** depicted band gap of TiO_2 NPs is 3.32 eV [21].

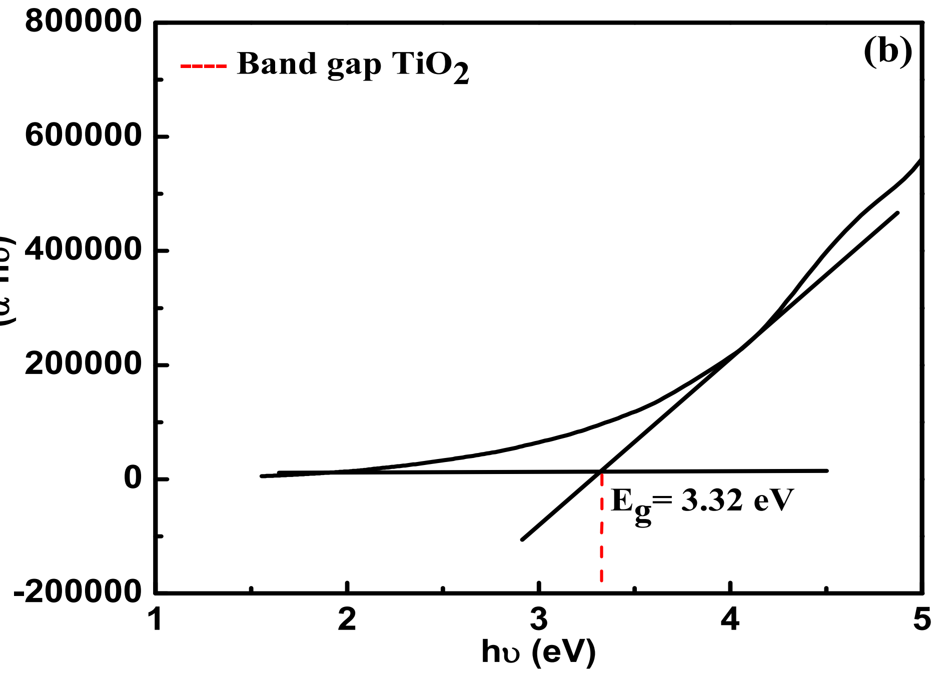

Fig. 2 (b) Optical band gap of TiO_2

3.2.2.FTIR

The FTIR spectroscopic results of CFE and biologically synthesized TiO_2 NPs depicted in **Fig. 3.** It also provides information about functional groups involvement in capping process. The peak at 1422 cm^{-1} to 1401 cm^{-1} indicates the C-N stretching present in *bacterial* proteins [22] shown in **Fig. 3. (a).** The distinct peaks are observed in TiO_2 NPs at 3427 cm^{-1}, 2924 cm^{-1}, 1652 cm^{-1} and 684 cm^{-1} shown in **Fig. 3 (b).** The peak at 3427 cm^{-1} due to N-H stretching band present in *Bacillus halodurans* containing protein. The band at 2924 cm^{-1} could be due to capped NPs confirms the bound carboxylic groups with Ti-O-Ti [23]. The peak at 1652 cm^{-1} shows characteristics of amide stretching along with N-H bending. The C-O ether linkage shown at peak 1020 cm^{-1}. The 684 cm^{-1} observed peak is due to Ti-O-O bond vibrations [24].

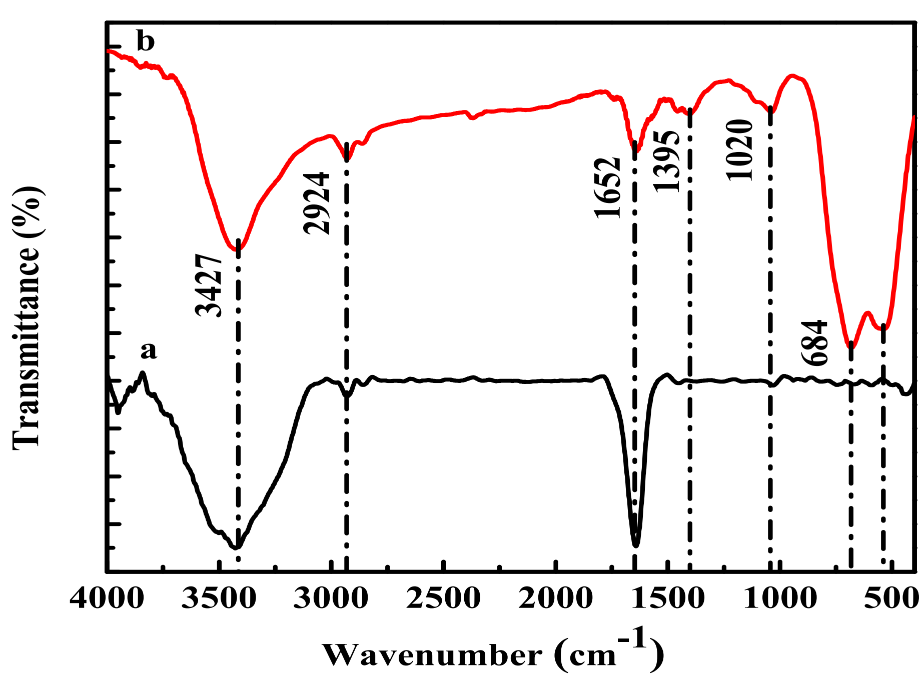

Fig. 3.Fourier transform infrared spectroscopy

- **(a) -Cell free extract (CFE)**
- **(b) -CFE mediated TiO_2 NPs.**

3.2.3. XRD

Fig.4. showed the biologically prepared TiO_2 NPs crystallographic information using XRD technique. The highly intense sharp peak of TiO_2 is well matched with JCPDS card No. 73-1764 which substantiate anatase stage of TiO_2. Debye Scherrer's equation is generally employed to calculate crystallite size of TiO_2 [25].

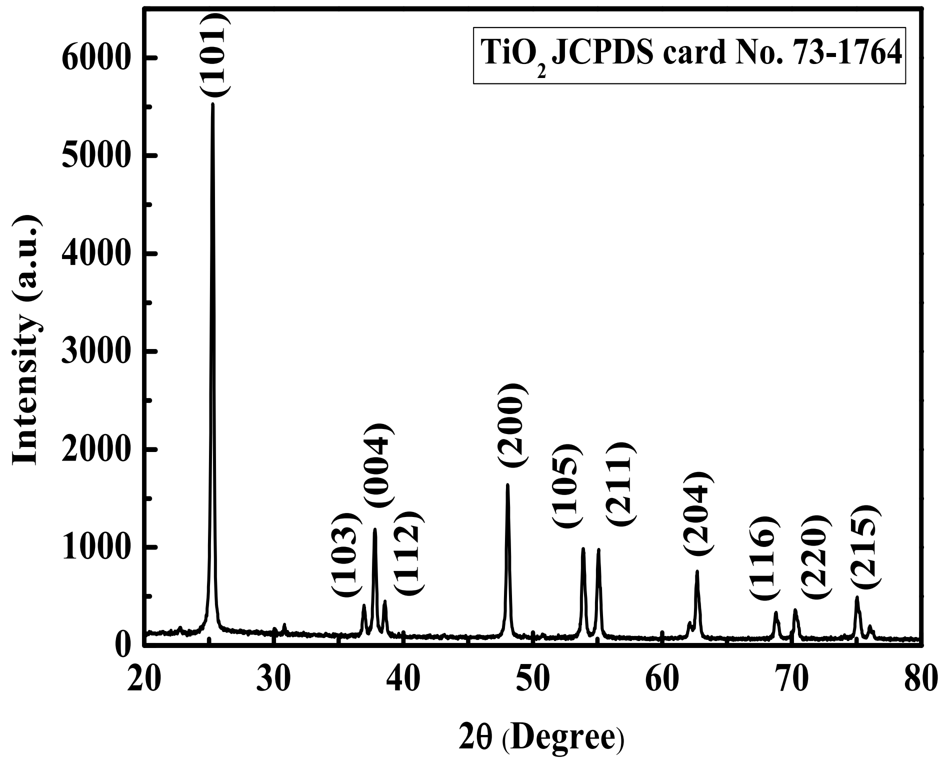

Fig. 4.X-ray diffraction (XRD) pattern of Anatase TiO_2NPs

3.2.4.TEM and BET study

The TiO_2 NPs shown spherical morphology having average size 33 nm in **Fig. 5 (a) (b).** The ordered white cluster discrete spots demonstrates the fine single crystalline nature of NPs in **Fig. 5 (c).** The lattice structure shown in **Fig. 5 (d).**

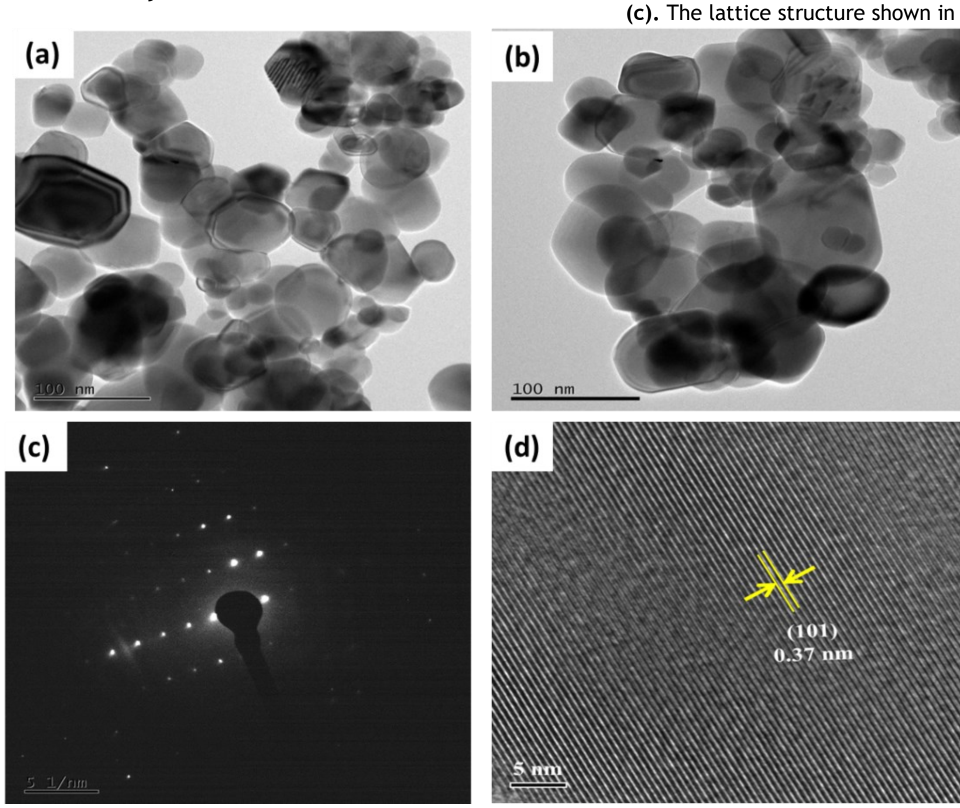

Fig. 5 (a) and (b) Transmission Electron Micrograph TiO_2 NPs., (c) White array discrete spots indicate the good single crystalline nature TiO_2 NPs., (d) Lattice spacing of TiO_2 NPs.

Porosity is a key factor in photocatalysis, and it is usually quantified using the renowned and advancing technique BET. **Fig. 6 (a).** Indicates. BET N_2 adsorption-desorption isotherm plot and **Fig 6 (b).** Indicates BJH plot utilized to gauge surface area and porosity of TiO_2NPs. The estimation of porosity alongside surface area of nanomaterial play a noteworthy part in photocatalytic textile dye degradation application for treatment industrial wastewater. As a result of high specific surface area of catalyst adsorb more number of reactive molecules on the othe hand highlights presence of more number of surface active sites. This results the photocatalytic degradation process to be more efficient [26].The calculated specific surface area of synthesized TiO_2NPs was 13.0665 m^2/g. Mesoporous nanostructure is confirmed by pore radius of anatase TiO_2 is 7.4092 nm which is in between 20 to 50 nm.

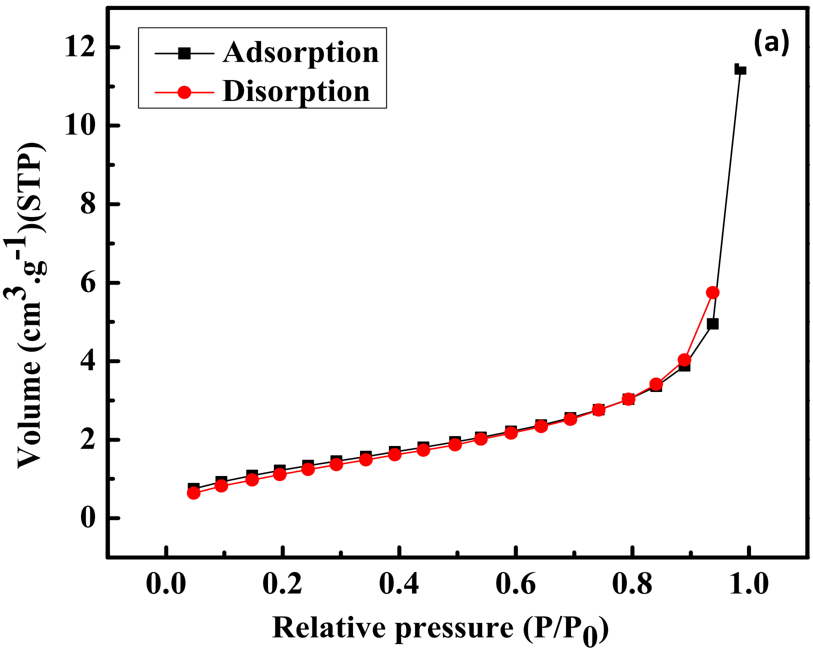

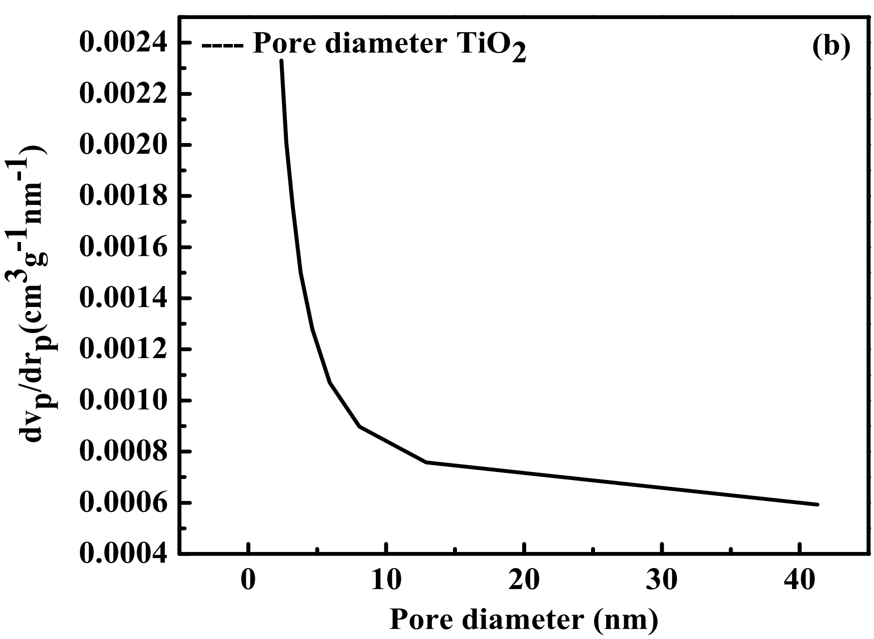

Fig. 6 (a) Branauer-Emmett-Teller (BET)N_2 adsorption-desorption isotherm plot, (b) Barrett-Joyner Halenda (BJH) plot

3.3. Photocatalytic activity of TiO_2 NPs

Different NPs used for dye degradation on the basis of photocatalytic activity principle. In our research we observed the photocatalytic activity of fungus mediated TiO_2 NPs. The catalytic activity of biosynthesized TiO_2 NPs was studied under sunlight, and using a UV-Vis spectrophotometer as shown in **Fig. 7 (A).** Red HE3B dye shown maximum absorbance at 510 nm [27, 28]. Addition of TiO_2NPs into Red HE3B dye mixture gradual decolorization of dye took place and color of the solution changed from blue to colorless within 30 min. A progressive decline in peak intensity maximum at 510nm was detected during the reduction reaction within a short time (30 min). Decline peak intensity indicates degradation of Red HE3B. The Surface Plasmon Resonance (SPR) crest for TiO_2 NPs was not observed in UV-visible spectrum during catalytic study. The biosynthesized TiO_2 NPs showed 99% Red HE3B degradation in the presence sunlight within 30 min in **Fig. 7 (B).** The reduction reaction was follow pseudo-first-order kinetics. The value of calculated rate constant (K_{app}) was analysed to be 0.1976 min^{-1} shown in **Fig. 7 (C).**

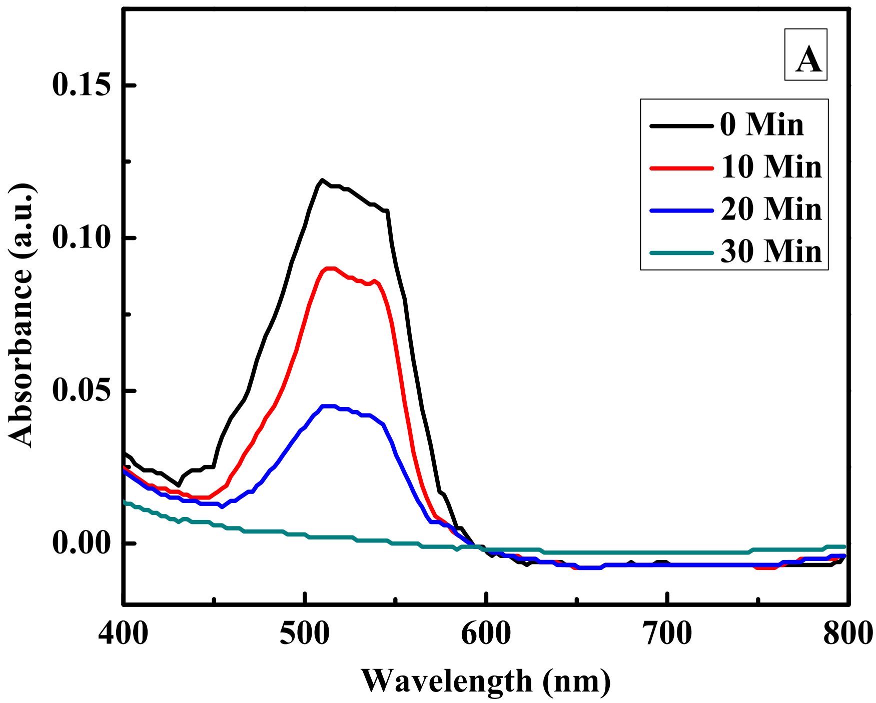

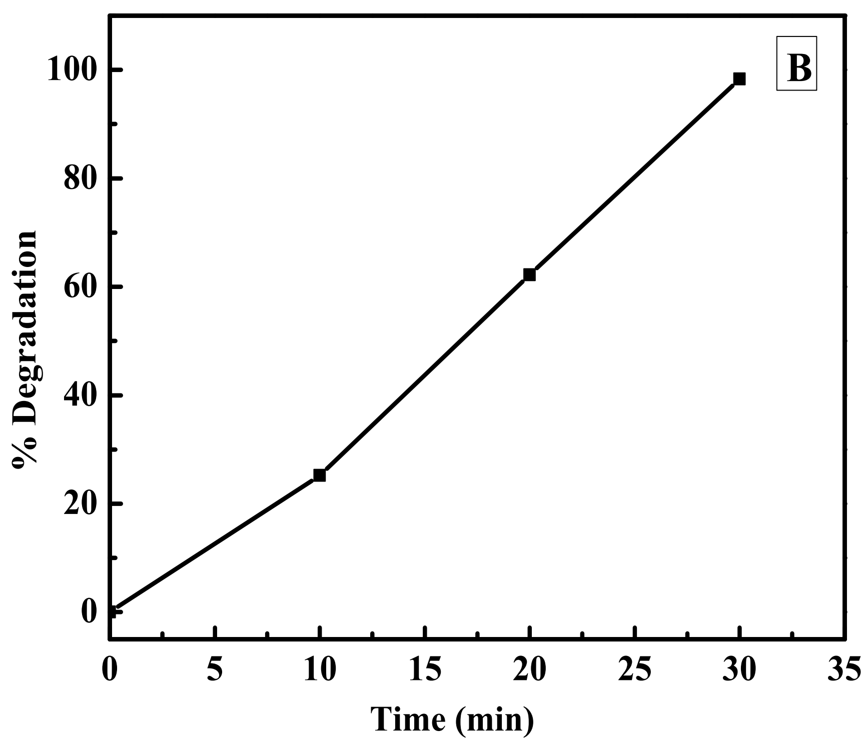

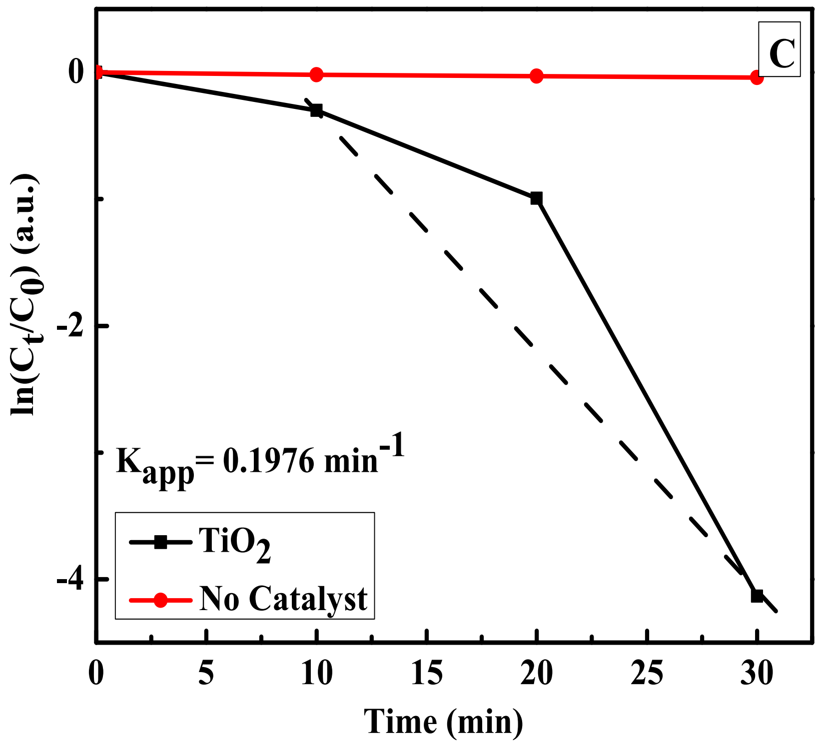

Fig. 7 (A) UV-Visible Absorption spectra of Red HE3B dye using TiO_2NPs at various time intervals, (B) Degradation % of Red HE3B dye with time in presence of TiO_2 material., (C) ln (Ct/Co) verses degradation time plot for finding the reaction rate constant (k_{app}).

3.4. Degraded Metabolites study

3.4.1. UV-Vis Spectroscopy

UV-Visible spectrophotometric analysis use to confirm degradation of Red HE3B was due to green synthesized TiO_2 nanoclusters display in **Fig. 7 (A).** The complete disappearance of 510 nm absorbance peak of Red HE3B dye indicates degradation is attributed due to TiO_2 NPs driven photocatalytic activity [29].

3.4.2. Thin-layer chromatography (TLC)

TLC analysis showed in **Fig. 8**, appearance of single spot of Red HE3B at 0 h (control), two spots arises in co-sample at two different positions shown in **Fig. 8 (c),** and appearance of single spot of degraded sample in **Fig. 8 (b),** indicates complete degradation of Red HE3B within 30 min. Control appearance only single spot with Retardation factor (RF) value observed at (0.96) in **Fig. 8 (a),** and product formed after 30 min degradation RF value 0.84 at pH 7.0.

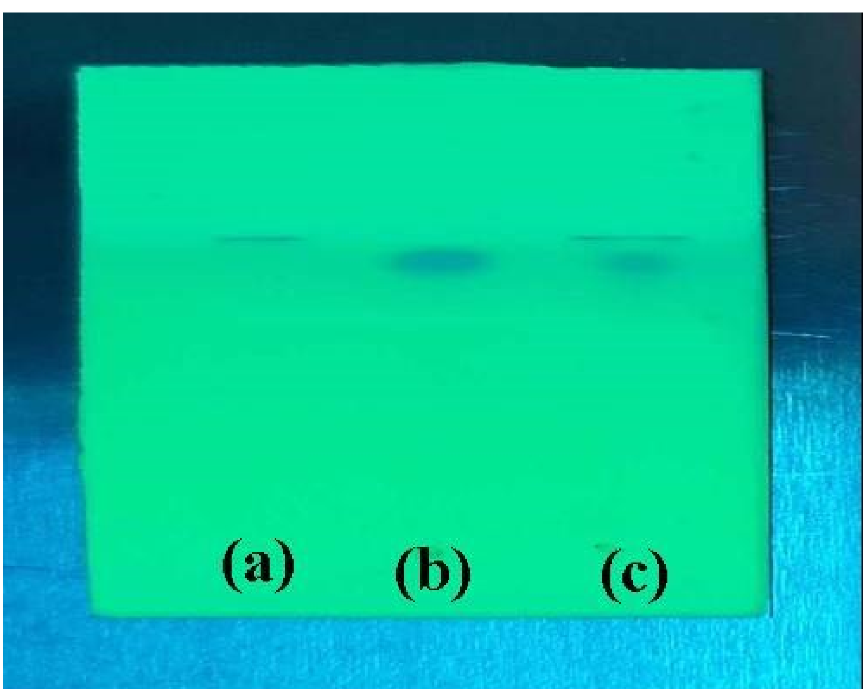

Fig. 8 (a)- Pure Red HE3B dye, (b)- Degraded metabolite, (c)- Pure Red HE3B dye with degraded metabolites (co-sample)

3.4.3. Fourier transforms infrared spectroscopy (FTIR)

FTIR analysis Red HE3B and samples extracted after dye degradation experiment proved bioremediation of dye into different metabolites driven by activity of TiO_2 NPs is shown in **Fig. 9.** The FTIR spectroscopic study of Red HE3B showed the various peaks arising at 3421 cm^{-1} and 2932 cm^{-1} showed single alcoholic bridge in CH stretch and CH stretch of asymmetric alkanes respectively. Peak at 1480 cm^{-1} indicate C=C stretching of disubstituted aromatic compounds. Peak at 1216 cm^{-1} showed S=O stretch for sulfur compounds. Peak at 1045 cm^{-1} for S=O sulfuric acid stretching. The FTIR spectrum of products formed after degradation i.e. test sample, showed peak at 3240 cm^{-1} for N=O nitrites stretching. Peaks at 2938 and 1450 cm^{-1} showed C-H stretching of asymmetrical alkanes groups. Peak at 1632 cm^{-1} indicates C=C stretching of aromatic groups. 1367 cm^{-1} displayed for S=O stretching of sulphur consisting compound. Peaks at 1030 and 1108 cm^{-1} indicate C–OH stretching of primary alcohol and CH deformation of pyridine respectively. FTIR spectrum of pure dye and degraded dye formed metabolites peaks, were significantly different [14].

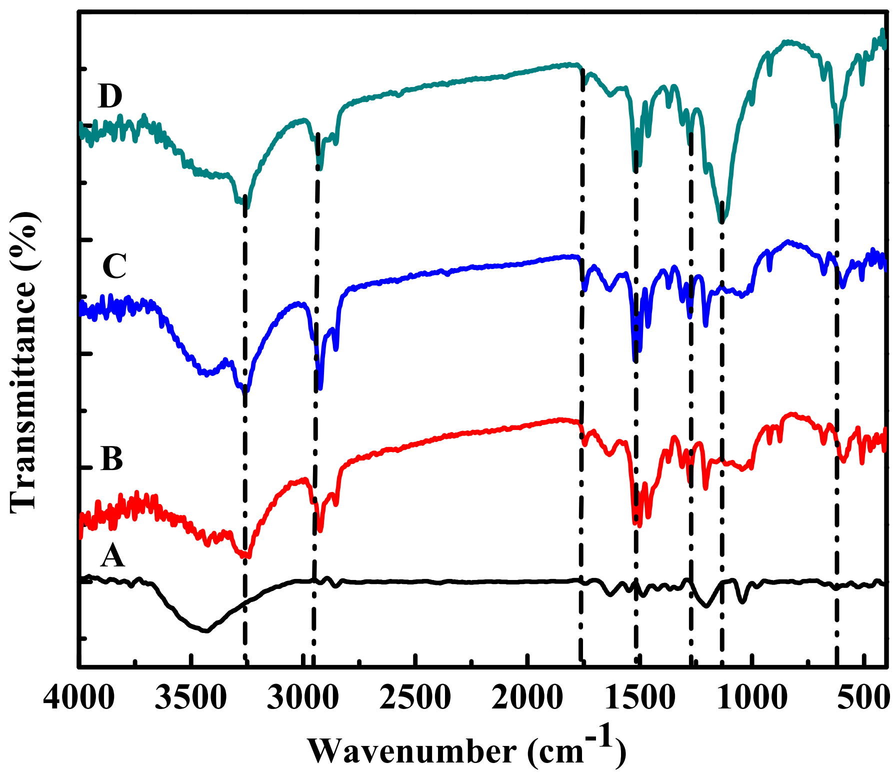

Fig. 9 A-Red HE3B dye control, B- Degradation after 10 min, C-Degradation after 20 min, D- Degradation after 30 min

3.4.4. High performance liquid chromatography (HPLC)

HPLC chromatograph of pure dye and the products produced after nanoremediation using TiO_2NPs, observed at 270 nm. The HPLC chromatogram of Red HE3B pure dye showed a intense peak at retention time 1.623 and 3.628 min in **Fig 10 (A)**. The metabolites generated after degradation shifting pure dye peak and appearance of various peaks at different retention times 2.612, 2.729 and 4.017min in **Fig. 10 (B). (C).** and **(D).** Respectively. HPLC analysis confirmed degradation of Red HE3B.

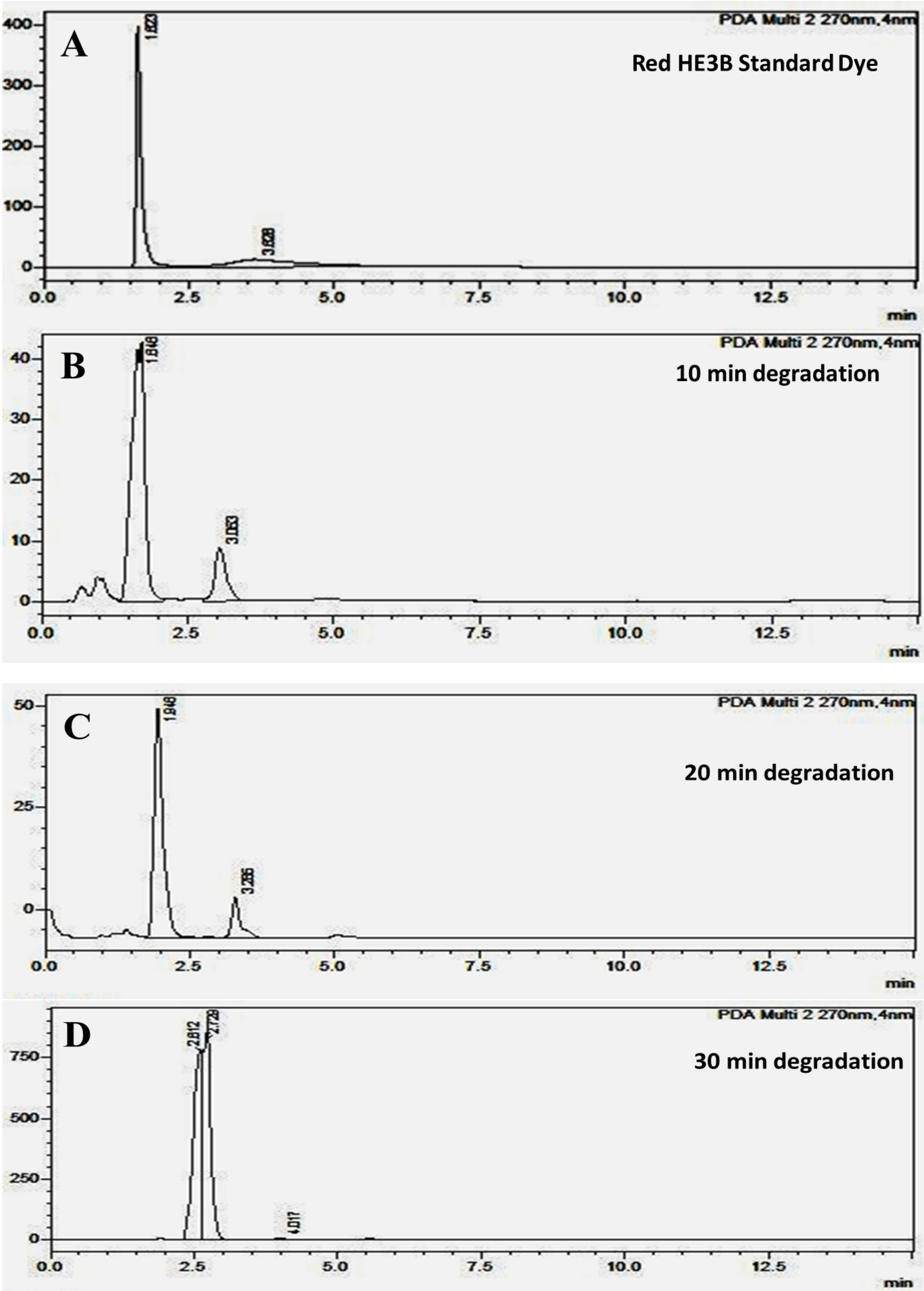

Fig. 10 A- Red HE3B dye control, B- Degradation after 10 min, C- Degradation after 20 min, D- Degradation after 30 min

3.4.5. LC-MS

On the basis of LC-MS obtained metabolites, we have predicted a degradation pathway of Red HE3B. LCMS results in **Fig. 11.** showed the mass spectra of degraded products formed after every 10 min time interval.

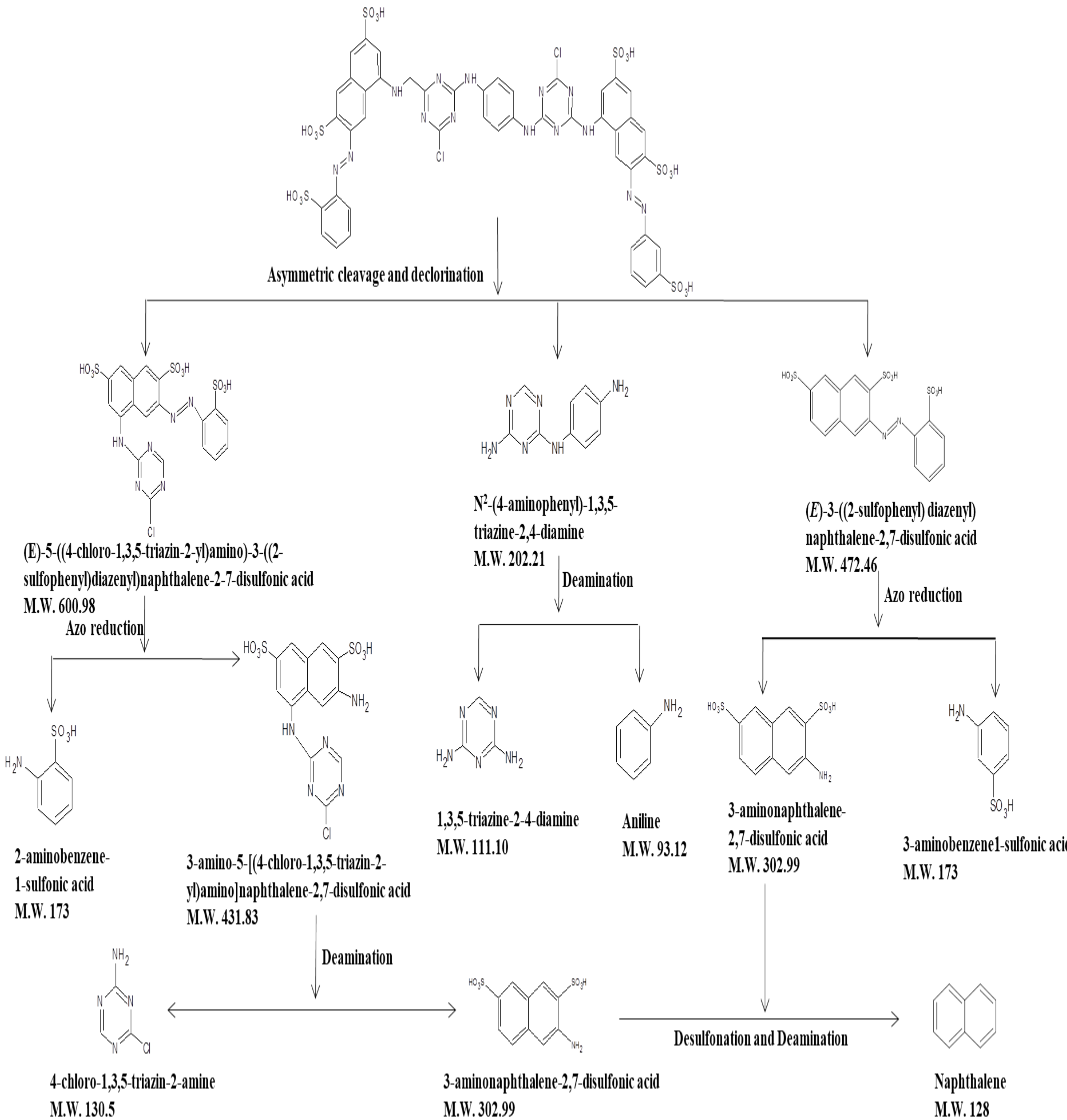

Fig. 11 Predicted biodegradation pathway of Red HE3B

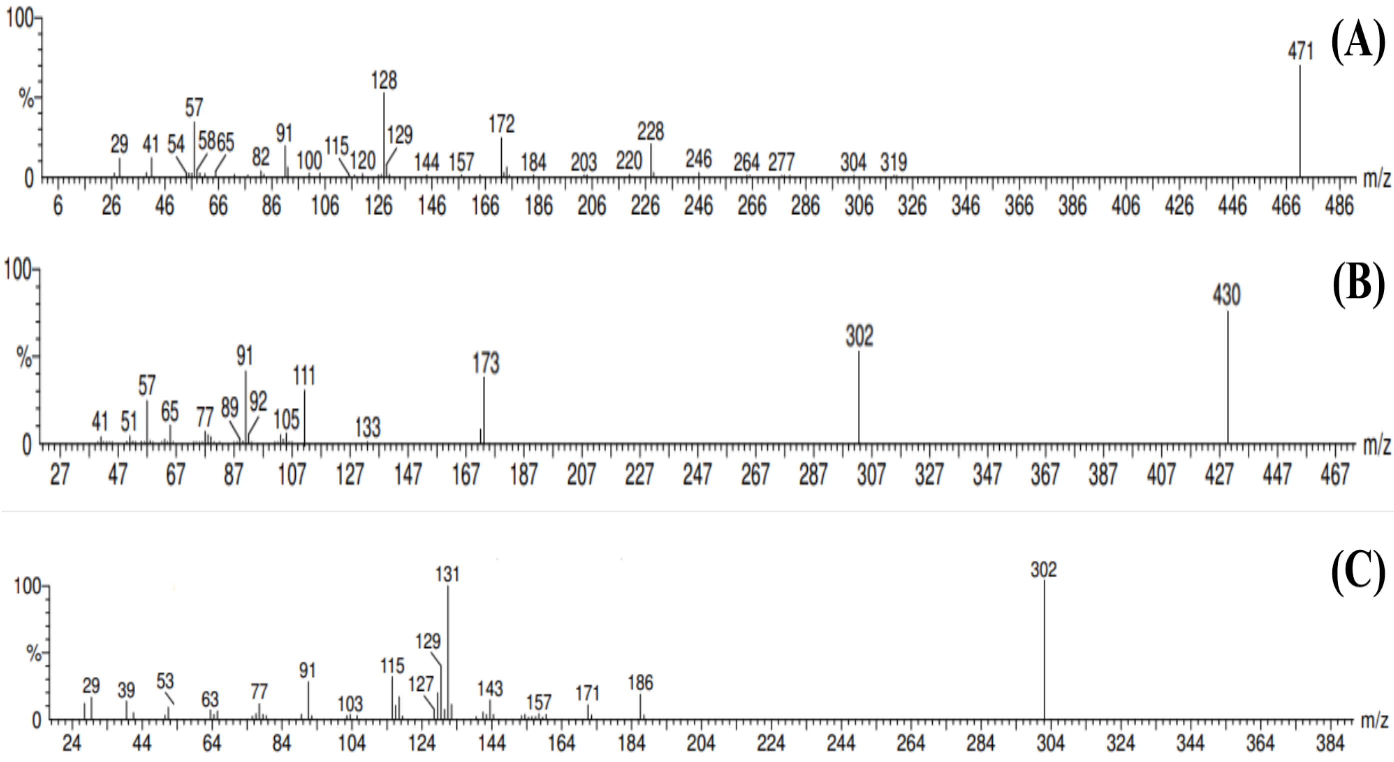

Fig. 11 Red HE3B dye A- Degradation after 10 min, B-Degradation after 20 min,C- Degradation after 30 min

3.5. Anticancer Studies

The in vitro cytotoxic effect of biosynthesized TiO_2 NPs was studied against Human breast adenocarcinoma MDA-MB-231 at various concentrations 25, 50, 100, 200 and 300 µg/ml. The significant reduction in cell viability of 73%, 52%, 32%, 15% and 8% with enhance concentration of TiO_2 NPs as mentioned above, within 48 h compared to untreated control shown in **Fig. 12 (A).** The MTT assay estimated IC-IC_{50}value was 56.41 µg/ml at 48 h showed in **Fig. 12 (B).** It revealed cytotoxic potent of TiO_2 NPs on MDA-MB-231cells in concentration dependent manner. Cancer cell uptake TiO_2 NPs possibly via endocytosis or passive diffusion and induces apoptosis and cytotoxicity [30]. NPs also interfere in signalling pathway epidermal growth factor receptor (EGFR) leading to cause stimulation of apoptosis pathway and inhibition of cell proliferation [31].

NPs inhibit intracellular antioxidant system pathway by trigger synthesis ROS and stimulate DNA damage leading to cause cell death [32, 33, 34, 35]. The overall results endorse that the synthesized TiO_2 NPs synthesized using *Bacillus halodurans* Kaas lake isolated bacteria exhibited high cytotoxic potential application in cancer therapy.

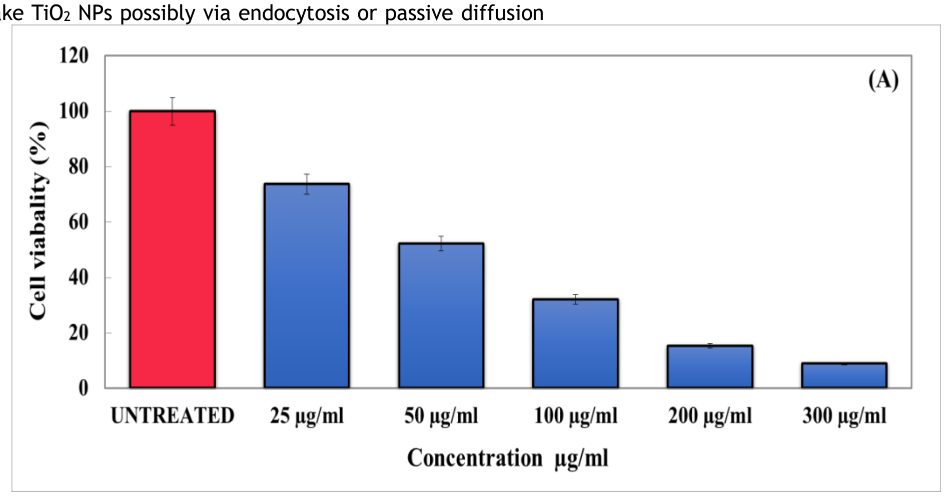

Fig. 12. (A)-. The figure represents the cytotoxic activity of biosynthesized TiO_2 NPs on viability in MDA-MB-231 cancer cells. The MDA-MB-231 cells were treated with TiO_2 NPs five different concentrations (25, 50, 100, 200 and 300 µg/ml) incubate at 48 h. Cytotoxicity increases with increase concentration of TiO_2 NPs. The data are presented as Mean ± SD and statistical significance is accepted at $p < 0.05$.

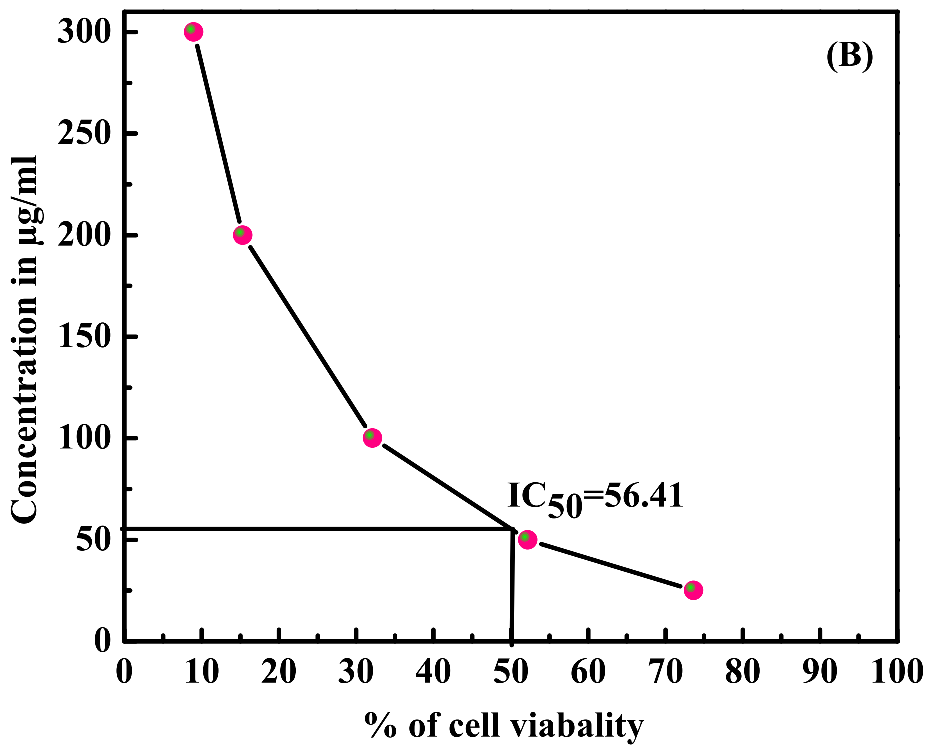

Fig. 12. (B)- IC_{50} value TiO_2 NPs 56.41µg/ml

3.5.1. Effect of TiO_2 NPs on MDA-MB-231 cells

The MDA-MB-231 cells showed fibroblast, aberrant, elongated spindle shape morphology. The increased TiO_2 NPs treated MDA-MB-231 cells showed stress and apoptosis after 48 h. The fibroblast and microvilli morphology of cancer cells began to lose, in addition to cytoplasmic vacuolation, cell blebbing, round and uneven shape confirms apoptosis cycle started. At 25 µg/ml concentration, the shrunk spindle shape was dominant, with small percentage of spherical shape of the cells shape. The spherical shape dominancy observed at higher concentrations of 200µg/ml and 300µg/ml with more toxicity. Only 8% cells exhibited almost lower spindle shapes after 48 h. incubation period. high concentration of TiO_2 NPs destructs the spindle shape more. About 92% of cancerous cells growth inhibited shown in **Fig. 12. (C).**

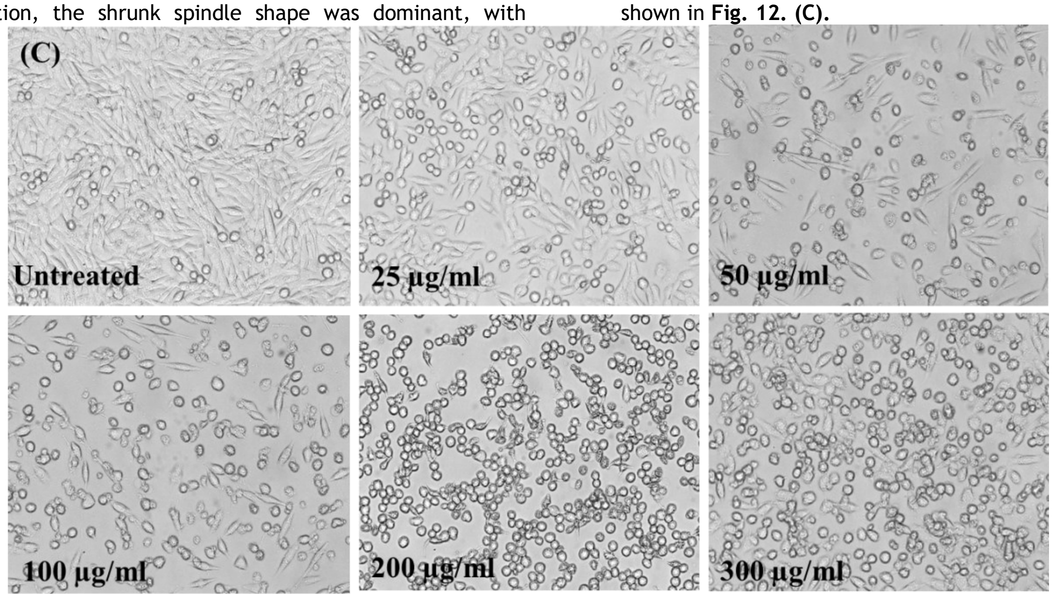

Fig. 12. (C)- The figure represents effects of TiO_2 NPs on morphology of MDA-MB-231 cells after treatment with five different concentrations (25, 50, 100, 200, 300 µg/ml) after 48 hours incubation. (C) Represents a zoom in for morphological changes caused by TiO_2 NPs on untreated cell shows- fibroblast-like shape. With increases the NPs concentration morphology of cell changes to uneven cell, cytoplasmic vacuolation and blebbing.

3.5.2. Statistical Analysis

TiO_2 NPs shown decrease in MDA-MB-231 cells proliferation with five different concentrations (25, 50, 100, 200, 300 µg/ml). The NPs treated cancer cells displayed significant inhibition in cell viability ($P < 0.05$) at all concentration after 48 h compared to untreated cells. However, the viability of breast cancer cells is dose concentration dependent manner showed in **Table.1. and Fig. 12. (C).**

Concentration of NPs.	Cell Viability (%)
UNTREATED	100 ± 0.03
25µg/ml	73.64 ± 0.01
50µg/ml	52.19 ± 0.01
100µg/ml	32.12 ± 0.02
200µg/ml	15.32 ± 0.01
300µg/ml	8.96 ± 0.01

Table.1. Statistical comparison: TiO_2 NPs various concentrations experimental set v/s control set. $P < 0.05$ showed significance difference

CONCLUSION

In conclusion, we reported simple, eco-friendly, cost effective approach for synthesis of spherical anatase TiO_2 nanospheres using bacteria. Phenotypic characterization and 16S r-RNA sequencing used to analyze isolated bacterial species. Synthesized material absorbance, phase confirmation was confirmed by using UV-DRS spectroscopy. XRD confirmed tetragonal crystaline structural arrangement of atom having average size 33 nm. The material shows excellent photocatalytic activity against Red HE3B dye 99.00% degradation within 30 min. Present work suggests that TiO_2 catalyst play significant role in production of ROS for dye degradation. The TiO_2 NPs showed significant in vitro cytotoxic potential on the MDA-MB-231 breast cancer cell line, with an IC-IC50 value of 56.41 µg/ml. The present research finding the prospective of TiO_2 NPs act smart materials to perform competently in environmental and biomedical applications. The multifunctional TiO_2 NPs act as better alternative for excellent photocatalytic activity and biomedical application for breast cancer theraphy. The development of a clean, nontoxic and environmentally compatible green way of generating metal oxide NPs utilizing microorganisms would be a boon in nanobiotechnology.

Declaration of Competing Interest

The authors declare that they have no known competing financial interests or personal relationships that could have appeared to influence the work reported in this paper.

Acknowledgments

One of the author, Avinash Survase, is grateful to the Council of Scientific and Industrial Research (CSIR), New Delhi, Government of India, for the award of the Junior Research Fellowship (File no. 09/1287(0001)/2019-EMR-I. Also, we thankful to Rayat Institute of Research and Development, Satara and Yashavantrao Chavan Institute of Science, constituent college of Karmaveer Bhaurao Patil University, Satara (Maharashtra, INDIA) for the laborotary support.

REFERENCES

- **[1]**H. B. Slama, C. Bouket, A. Pourhassan, Z. Alenezi, F.N. Silini, A. Cherif-Silini, H. Oszako, T. Luptakova, L. Golinska, P. Belbahri, Diversity of Synthetic Dyes from textile industries discharge impacts and treatment methods, Appl. Sci. 11 (2021) 1-21.
- **[2]**P. S. Patil, S. S. Phugare, S. B. Jadhav, and J. P. Jadhav, Communal action of microbial cultures for Red HE3B degradation, J. Hazard. Mater., 81 (2010) 263-270.
- **[3]**K. Dwivedi, G. Kumar, Genetic damage induced by a food coloring dye on meristematic cells of Brassica campestris L. J., Environ. Public Health, (2015) 1-5.
- **[4]**D. C. Martel, D. Georges, F. Bray, J. Ferlay, G. M. Clifford, A Global burden of cancer attributable to infections in 2018: a worldwide incidence analysis, Lancet Glob Health. 8 (2) (2020) 180-190.
- **[5]**A. Jemal, F. Bray, M. M. Center, J. Ferlay, E. Ward, D. Forman, Global cancer statistics., CA Cancer J. Clin. 61 (2011) 69-90.
- **[6]**D. Khezerloo, T. Mortezazadeh, B. Farhood, P. Sheikhzadeh, N. Seyfizadeh, L. Pezhman , The effect of date palm seed extract as a new potential radioprotector in gamma-irradiated mice., J Cancer Res Ther. 15 (3) (2019) 517-521.
- **[7]**R. Medhi, M.D. Marquez, T.R.Lee, Visible-light-active doped metal oxide nanoparticles: review of their synthesis, properties, and applications, ACS Applied Nano Materials, 3(7) (2020) 6156-6185.
- **[8]**L. Qianwen, A. Zhang, R. Wang, Q. Zhang, D. Cui, A review on metal-and metal oxide-based nanozymes: Properties, mechanisms, and applications, Nano-micro letters 13 (1) (2021) 1-53.
- **[9]**V. Gargiulo, M. Alfe, L. Giordano, S. Lettieri, Materials for Chemical Sensing: A comprehensive review on the recent advances and outlook using ionic liquids, metal–organic frameworks (MOFs), and MOF-based composites, Chemosensors 290 (10) (2022) 1-39.
- **[10]**S. Hongbo, R. Magaye, V. Castranova, J. Zhao, Titanium dioxide nanoparticles: a review of current toxicological data, Particle and fibre toxicology 10 (1) (2013) 1-33.
- **[11]**J. Riu, A. Maroto , F.X. Rius, Nanosensors in environmental analysis, Talanta, 69 (2) (2006) 288-301.
- **[12]**D. B. Warheit, T. R. Webb, K. L. Reed, S. Frerichs, C. M. Sayes, Pulmonary toxicity study in rats with three forms of ultrafine-TiO_2 particles: differential responses related to surface properties, Toxicology 230 (2007) 90-104.
- **[13]**M. Alavi, N. Karimi, T. Valadbeigi., Antibacterial, Antibiofilm, Antiquorum Sensing, Antimotility, and Antioxidant Activities of Green Fabricated Ag, Cu, TiO_2, ZnO, and Fe_3O_4 NPs via Protoparmeliopsis muralis Lichen Aqueous Extract against Multi-Drug-Resistant Bacteria., ACS Biomater Sci Eng. 9 (5) (2019) 4228-4243.
- **[14]** A. A. Survase and S. S. Kanase., Green synthesis of TiO2 nanospheres from isolated Bacillus halodurans No. AH-101 and its multifunctionality in nanobioremediation of CI Reactive Blue 194 with antimicrobial and antioxidant activity. *Ceramics International* 49, no. 10 (2023): 14964-14980.
- **[15]**A. P. Torane, A. B. Ubale, K. G. Kanade, P. K. Pagare, Photocatalytic dye degradation study of tio2 material, Mater. Today Proc, 43 (2020) 2738-2741.
- **[16]**R. Mata, J.R. Nakkala, S.R. Sadras, Biogenic silver nanoparticles from Abutilon indicum: their antioxidant, antibacterial and cytotoxic effects in vitro, Colloids Surf. B: Biointerfaces 128 (2015) 276-286.
- **[17]**S. Cassaignon, M. Koelsch, J. P. Jolivet, From $TiCl_3$ to TiO_2 nanoparticles (anatase, brookite and rutile): Thermohydrolysis and oxidation in aqueous medium,

Journal of Physics and Chemistry of Solids, 68 (2007) 695-700.

- **[18]**B. R. Mugundan, G. Viruthagiri, N. Shanmugam, R. Gobi, P. Praveen,Synthesis and characterization of undoped and cobalt-doped TiO_2 nanoparticles via sol–gel technique. Applied Nanoscience 5 (4) (2015) 449-456.
- **[19]**M. K. Peiris, T. Guansekera, P. M. Jayaweera, S Fernando, TiO_2 Nanoparticles from Baker's Yeast: A Potent Antimicrobia, J. Microbiol. Biotechnol 28 (10) (2018) 1664–1670.
- **[20]**T. Luttrell, S. Halpegamage, J. Tao, A. Kramer, E. Sutter, M. Batzill, Why is anatase a better photocatalyst than rutile? - Model studies on epitaxial TiO_2 films, Sci. Rep., 4 (2015) 1-8.
- **[21]**B.M. Babar, K. B. Pisal, S. H. Sutar, Hydrothermally Prepared VanadiumOxide Nanostructures for Photocatalytic Application, ES Energy Environ., (2022)82-91.
- **[22]**F. A. Saif, S. A. Yaseen, A. S. Alameen, S. B. Mane, P. B. Undre, Identification and characterization of Aspergillus species of fruit rot bacteria using microscopy, FT-IR, Raman and UV-Visspectroscopy, Spectrochim. Acta - Part A Mol. Biomol. Spectrosc., 246 (2021) 119010-119046.
- **[23]**A. Leon, P. Reuquen, C. Garin, R. Segura, P. Vargas, P. Zapata, P. A. Orihuela, FTIR and raman characterization of TiO_2 nanoparticles coated with polyethylene glycol as carrier for 2-methoxyestradiol, Appl. Sci., 7 (2017) 1-9.
- **[24]**P. Dhandapani, S. Maruthamuthu, G. Rajagopal, Bio-mediated synthesis ofTiO_2 nanoparticles and its photocatalytic effect on aquatic biofilm, J. Photochem. Photobiol. B. Biol., 110 (2012) 43-49.
- **[25]**L. Yao, W. B. Yu, B. X. Xu, New insight into the interface of TiO_2/C as nanocomposite electrode for lithium-ion batteries, Journal of Power Sources 534 (2022): 231406.
- **[26]**G. K. Upadhyay, V. Kumar, L. P. Purohit, Optimized CdO:TiO_2 nanocomposites for heterojunction solar cell applications, J. Alloys Compd., 856 (2020) 1-14.
- **[27]**K. Sathiyan, R. Bar-Ziv, O. Mendelson, T. Zidki, Controllable synthesis ofTiO_2 nanoparticles and their photocatalytic activity in dye degradation, Mater. Res.Bull., 126, (2019) 110842-110850.
- **[28]** H. D. Shelke, A.R. Machale, A. A.Surwase, S. F. Shaikh, A. U. H.S. Rana and H. M. Pathan, Enhanced photocatalytic activity of the Cu2SnS3+ GO composite for the degradation of navy blue ME2RL industrial dye. Coatings, 13(3), (2023) 522.
- **[29]**B. M. Babar, K. B.Pisal, S. H. Mujawar, V. L.Patil, L. D.Kadam, U. T.Pawar, P. M. Kadam, P. S.Patil, Concentration modulated vanadium oxide nanostructures for NO_2 gas sensing, Sensors and Actuators B: Chemical, 351 (15) (2022):130947.
- **[30]**C. Liao, Y. Li, T. S. jong, Visible-light active titanium dioxide nanomaterials with bactericidal properties., Nanomaterials (Basel) 10 (1) (2020) 1-56.
- **[31]**H. Kim, D. Jeon, S. Oh, K. Nam, S. Son, M. Gye, I. Shin, Titanium dioxide nanoparticles induce apoptosis by interfering with EGFR signaling in human breast cancer cells., Environmental Research 175 (2019) 117-123.
- **[32]**E. Galata, E.A. Georgakopoulou, M.E. Kassalia, F. N. Papadopoulou, E.A. Pavlatou , Development of smart composites based on doped-TiO_2 nanoparticles with visible light anticancer properties. Materials (Basel) 12 (16) (2019) 2585-2589.
- **[33]** S. S. Wagh, A. S. Chougale, A. A. Survase, R. S. Patil, N. Naik, M. Naushad, H. M. Pathan, Rapid photocatalytic dye degradation, enhanced antibacterial and antifungal activities of silver stacked zinc oxide garnished on carbon nanotubes, Scientific Reports, 14 (1) (2024) 14045.
- **[34]** A. A. Survase, S. S. Kanase, Novel microbial synthesis of rGO nanosheets for effective photocatalytic remediation of Acid Blue 113 dye, improved seed germination, antimicrobial and antioxidant applications. Journal of Molecular Structure, 1302 (2024), 137421.
- **[35]** A. D. Kadam, A. C. Sapkal, A. A. Survase, S. B. Kamble, Aspergillus Oryzae Mediated α-Fe2O3 Nanoparticles for Photocatalytic Remediation of Basic Fuschin Dye and Antimicrobial Activities. Chemistry Select, 9 (20), (2024) 202400088.